DNA Nanotechnology | Hot Paper

DOI: 10.1002/anie.201408941

Reversible Reconfiguration of DNA Origami Nanochambers Monitored by Single-Molecule FRET**

Barbara Saccà, Yuji Ishitsuka, Rebecca Meyer, Andreas Sprengel, Elisa-Charlott Schöneweiß, G. Ulrich Nienhaus,* and Christof M. Niemeyer**

Abstract: *Today, DNA nanotechnology is one of the methods of choice to achieve spatiotemporal control of matter at the nanoscale. By combining the peculiar spatial addressability of DNA origami structures with the switchable mechanical movement of small DNA motifs, we constructed reconfigurable DNA nanochambers as dynamic compartmentalization systems. The reversible extension and contraction of the inner cavity of the structures was used to control the distance-dependent energy transfer between two preloaded fluorophores. Interestingly, single-molecule FRET studies revealed that the kinetics of the process are strongly affected by the choice of the switchable motifs and/or actuator sequences, thus offering a valid method for fine-tuning the dynamic properties of large DNA nanostructures. We envisage that the proposed DNA nanochambers may function as model structures for artificial biomimetic compartments and transport systems.*

The invention of the DNA origami method has revolutionized our approach to the nanosized world, providing a powerful means to control spatial organization of matter at the nanometer length scale.[1] This bottom-up approach relies on the folding of a long single-stranded DNA into a desired shape by the help of hundreds of complementary predesigned short "staple" oligonucleotides. As the staples are uniquely defined and the position of their nucleobases within the DNA structure is exactly known, the origami method offers the extraordinary possibility to address a roughly ten thousand nanometer square surface with sub-nanometer precision, thereby paving the way to numerous applications which were previously barely imaginable.[2] Modern single-molecule technologies, in particular fluorescence-based methods, are contributing to the further advancement of DNA nanotechnology, because of their ability for nondestructive in situ studies with superior time resolution of a few milliseconds.[3]

Despite the enormous progress made, major efforts have so far been focused mainly on the use of DNA nanostructures as static platforms for the observation and manipulation of molecular events.[4] However, as nature teaches us, tight control of cellular processes is often associated with dynamic systems, capable of reversibly altering their configuration in response to environmental changes. Notable examples are biological compartmentalization systems, such as protein cages,[5] viral capsids,[6] lipid vesicles,[7] and bacterial microcompartments.[8] Inspired by their natural counterparts, several examples of DNA cages have been reported for encapsulation and delivery applications,[9] and in some cases their reversible reconfiguration has also been demonstrated.[10] However, since these polyhedral architectures usually lack the structural diversity and anisotropic addressability typical of DNA origami, an implementation of dynamic properties into large origami-based compartmentalization systems would be desirable. Until now, this issue has only been partially addressed, because structural reconfiguration of large origami constructs mostly resulted in irreversible transformation between topologically different shapes[11] or the transduction of such configurational changes to potential cargos remained unexplored.[12] Therefore, the creation and exploitation of truly bio-inspired compartmentalization devices that enable both precise spatial confinement and reversible dynamics of cargos remain a challenging task.

Here, we describe the completely reversible reconfiguration of quasiplanar DNA origami nanochambers, triggered by the controlled extension and/or contraction of switchable

[*] Dr. B. Saccà,[+] A. Sprengel, E. C. Schöneweiß
Center for Nanointegration Duisburg-Essen (CENIDE) and Center for Medical Biotechnology (ZMB)
University of Duisburg-Essen
Universitätsstrasse 2, 45117 Essen (Germany)
E-mail: barbara.sacca@uni-due.de

Dr. Y. Ishitsuka,[+] Prof. G. U. Nienhaus
Institute of Applied Physics
Karlsruhe Institute of Technology (KIT)
Wolfgang-Gaede-Strasse 1, 76131 Karlsruhe (Germany)
E-mail: uli.nienhaus@kit.edu

Dr. R. Meyer, Prof. C. M. Niemeyer
Institute for Biological Interfaces (IBG 1)
Karlsruhe Institute of Technology (KIT)
Hermann-von-Helmholtz-Platz 1
76344 Eggenstein-Leopoldshafen (Germany)
E-mail: niemeyer@kit.edu

Prof. C. M. Niemeyer
Institute for Toxicology and Genetics (ITG)
Karlsruhe Institute of Technology (KIT)
Hermann-von-Helmholtz-Platz 1
76344 Eggenstein-Leopoldshafen (Germany)

Prof. G. U. Nienhaus
Department of Physics, University of Illinois at Urbana-Champaign
Urbana, IL 61801 (USA)

[+] These authors contributed equally to this work.

[**] This work was supported by the Mercator Stiftung (Pr. 2011-0004) and the CRC 1093 initiative of the DFG (Pr. A6) to B.S., Ni291/9-1 and KIT in the context of the Helmholtz STN program to GUN, and Ni399/10-2 to C.M.N. We thank Kathrin Jeske for experimental help in AFM imaging.

Supporting information for this article is available on the WWW under http://dx.doi.org/10.1002/anie.201408941.

 © 2015 Wiley-VCH Verlag GmbH & Co. KGaA, Weinheim

hinges in the structure. The conformational transformation alters the size of an inner cavity within the origami construct, thereby enabling a reversible change in the distance between two distinct payloads. By using single-molecule FRET measurements we demonstrate that the energy transfer between two internalized fluorophores can be dynamically controlled by switching the conformation of the scaffold. Moreover, the kinetics of the process are strongly affected by the choice of the switchable motifs and/or actuator sequences.

Origami nanochambers were prepared from single-stranded DNA from the M13mp18 virus. The DNA was folded into rectangular structures about 90 nm in length × 65 nm in width, with an internal cavity of about 20 nm × 20 nm (Figure 1). As in most planar DNA origami structures, the circular folding path of the scaffold divides the shape into two halves, which are joined together by staple sequences spanning adjacent edges of a common seam. The seam sequences of the rectangular structures were designed to contain internal hairpin regions that were 15 bases long and made up of a 5 bp stem (C_5G_5) and a T_5 loop (see Figure S1 in the Supporting Information). Hybridization of the hairpin sequences of the seam with a fully complementary DNA strand (herein referred to as "fuel") leads to formation of a more-stable 15 bp long double-helical domain. The conformational transition from the compact hairpin (closed state) to the extended double helix (open state) results in a linear extension of about 5 nm along the helical axes of the origami, thereby increasing the size of the inner cavity (Figure 1).

We designed two types of nanochambers, whose functioning, although driven by the same DNA-hybridization mechanism, resembles either a tweezer-like (Figure 1 a) or a plug-like (Figure 1 b) movement. The difference in the operational mode of the two devices is caused by the absence (tweezer) or presence (plug) of an unpaired region of the scaffold strand on the upper side of the origami structure. In the tweezer, the contiguity of the scaffold pairing in the first helical domain of the origami is responsible for keeping the upper two halves of the structure firmly anchored to one another. The remaining 281 unpaired nucleotides of the scaffold are located at the bottom of the seam (magenta region in Figure 1 a), thus allowing the two lower parts of the device to move apart upon addition of DNA fuels. In contrast, the plug nanochamber contains two unpaired regions located at both ends of the seam, thus providing the two halves of the structure with a higher degree of motional freedom (140 bases and 141 bases at the top and bottom, respectively, of the structure; Figure 1 b). Reversible switching of the devices is achieved by opening the origami's internal hairpins with a fuel strand (orange in Figure 1) and closing by addition of a fully complementary "antifuel" strand (green). The conformational switching was found to be fully reversible for several consecutive cycles (Figure 2, see also Figures S2–S4 in the Supporting Information).

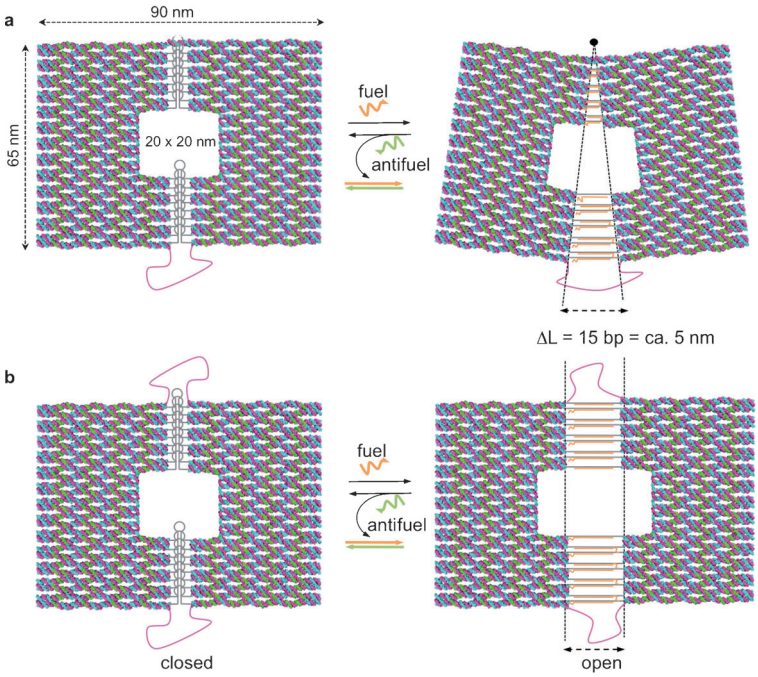

Figure 1. Switchable tweezer (a) and plug (b) DNA origami devices. The two halves of the devices are joined by hairpin motifs at the seam and a long unfolded region of the scaffold at the bottom extremity. The absence or presence of an unpaired scaffold segment on the upper side of the origami structures defines the operational mode of the device, respectively, as a tweezer (a) or a plug (b). The DNA-induced conformational transition of the hairpin motifs to extended double helices is driven by addition of complementary "fuel" strands (in orange), thus resulting in an about 5 nm increase in the length of the internal cavity along the direction of the helical axes (open state). Switching back to the initial closed state is achieved using toehold-appended fuels followed by addition of fully complementary antifuels (in green). Reversible switching of the devices leads to production of double-helical "waste" strands at the end of each cycle.

The origami structures were analyzed by gel electrophoresis, atomic force microscopy (AFM), and single-molecule FRET. Gel electrophoresis revealed that both the closed (C) and open (O) states of the devices migrate as a single well-defined band and the two species revealed only minimal differences in their electrophoretic mobility (Figure 2, upper gel). Fluorescently labeled fuel strands were used to clearly demonstrate the opening and closing of the device through the presence or absence, respectively, of a fluorescent band (Figure 2, lower gel panel). Reversibility of switching was demonstrated for both the tweezer and plug devices for up to three consecutive cycles, without any apparent decrease in the cycling efficiency of either system (see Figure S2 in the Supporting Information).

AFM analyses of the devices revealed that both the tweezer (Figure 3 a) and the plug (Figure 3 d) were formed in quantitative yields. Close inspection of the images revealed the double-helical features generated upon addition of the fuels along the central seam (Figure 3 b,e).

In accordance with theoretical estimations, statistical analysis of several high-resolution AFM images revealed a maximal increase in the length of the open structures of about 5 nm (see Figure S5 in the Supporting Information). To further visualize the presence of hybridized fuel strands inside the

 © 2015 Wiley-VCH Verlag GmbH & Co. KGaA, Weinheim

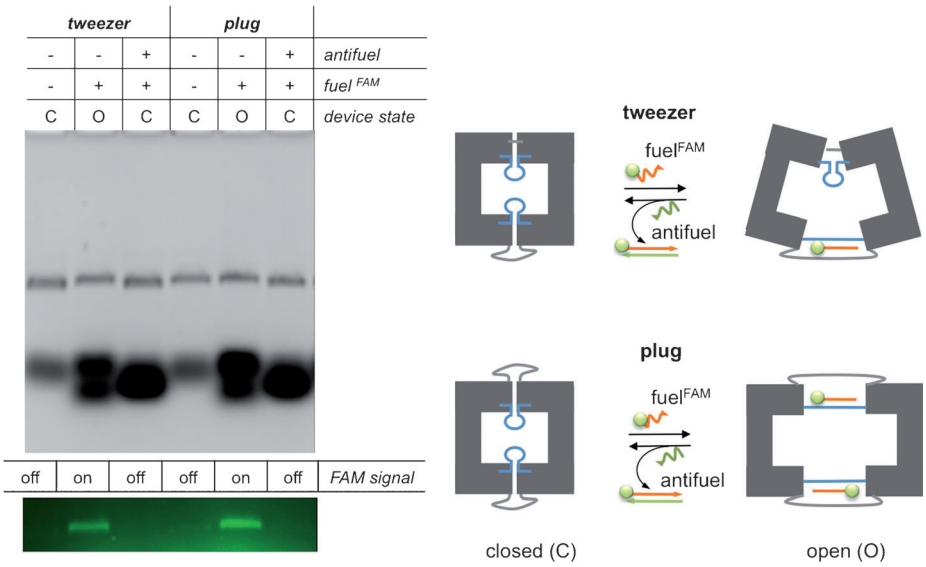

Figure 2. Gel electrophoresis characterization of tweezer and plug function using fluorescently labeled fuels. Both the closed (C) and open (O) states of the tweezer (lanes 1–3) and plug (lanes 4–6) devices migrate as single and well-defined products. Only minimal differences in the migration rate of the species are observable (upper gel). Labeling the opening fuel strands with fluorescein (fuel^{FAM}, in orange) allows the mechanical opening process to be coupled with a fluorescence signal (lower gel). On and off optical switching may be achieved by using suitable toehold sequences followed by the addition of fully complementary antifuels (in green). Gel conditions: 0.75% agarose in 1x TBEMg, 80 V, 3 h, 4 °C; detection with a fluorescein filter and UV illumination before and after staining with ethidium bromide.

origami structures, we used biotinylated fuel strands and streptavidin (STV) molecules as topographical markers. As expected, the STV molecules were clearly visible as bright spots located at the central seam (Figure 3c,f). Disappearance of streptavidin markers after addition of antifuels, demonstrated the reversible cycling of the devices (see Figures S3 and S4 in the Supporting Information). The opening and closing yields, as monitored by AFM, were almost 100% for both devices and processes, using different fuel/antifuel systems (see Figures S3 and S4 in the Supporting Information).

Single-molecule FRET microscopy was used to monitor the dynamics of the plug operation. To this end, a 64 bp long duplex bearing a central hairpin loop with the same sequence as those inserted in the seam of the origami structure and flanked by a Cy3-Cy5 pair was installed in the cavity of the plug nanochamber (Figure 4a and see Figure S6 in the Supporting Information for design details). The length of the duplex bridge was designed to match exactly the distance between the two opposite inner sides of the chamber to minimize the generation of tensile strain within the structure. In this way, the mechanical response of the device to fuel addition was expected to be unaffected by the presence of the bridge, and the inner labeled loop could, therefore, be used as a reporter of the translational movement of the entire system. Single-molecule FRET experiments were carried out with samples immobilized through avidin–biotin interactions on glass slides coated with polyethylene glycol. To this end, the origami structures were tagged with biotin molecules only at the left-side edge to maintain conformational freedom for the translational movement along the origami's x-axis (Figure 4a). Experiments were performed on four sets of plug devices (Figure 4b, see also Figures S7–S9 in the Supporting Information). Besides the original construct (I, Figure 4b), the effect of loop length (II, see Figure S7 in the Supporting Information) and fuel sequences (III and IV, see Figures S8 and S9 in the Supporting Information) on the kinetics of the opening/closing process were investigated.

For all the systems analyzed, inspection of the FRET population distribution at regular time intervals revealed a homogeneous response, that is, most of the devices underwent the structural reconfiguration swiftly, as indicated by the appearance of one major and relatively narrow FRET peak at each time point (Figure 4b and see Figures S7–S9 in the Supporting Information). Moreover, the closed-to-open transition was complete and resulted in a FRET efficiency variation of approximately 60%, with the values centered on 0.67 ± 0.07 (closed; Figure 4b, left panel) shifting to 0.12 ± 0.10 (open; Figure 4b, center panel and see Figures S7a–S9a in the Supporting Information). For the Cy3-Cy5 fluorophore pair (Förster radius $R_0 = 5.6$ nm),[13] this corresponds to a donor–acceptor distance change of about 4 nm (ca. 12 bp), which is in good agreement with the expected translational extension induced by the hairpin-to-duplex formation. Notably, the reconfiguration process was reversible in all the constructs analyzed, as evident by the reappearance of the high FRET peak at around 0.7 associated with the reclosed state upon addition of antifuel strands (Figure 4b, right panel, and see Figures S7b–S9b in the Supporting Information). Full reversibility could be observed even up to three consecutive cycles for construct IV (see Figure S10 in the Supporting Information). Only about 11% of the reclosed samples remained in the open conformation, possibly because of sterically inaccessible fuel strands, or fuel strands that lacked the flanking sequence for annealing antifuels. Consistent results were obtained by placing the fluorophore pair at slightly different positions of the inner bridge (see Figure S11 in the Supporting Information) and replacing the central bridge sequence by a random DNA sequence that does not anneal to the fuel strand (see Figure S12 in the Supporting Information). In addition, FRET distributions obtained on freely diffusing[14] DNA origami constructs were similar to those obtained on samples immobilized on surfaces (see Figure S13 in the Supporting Information). These data clearly indicate that the changes in FRET efficiency observed in all the constructs analyzed are

© 2015 Wiley-VCH Verlag GmbH & Co. KGaA, Weinheim

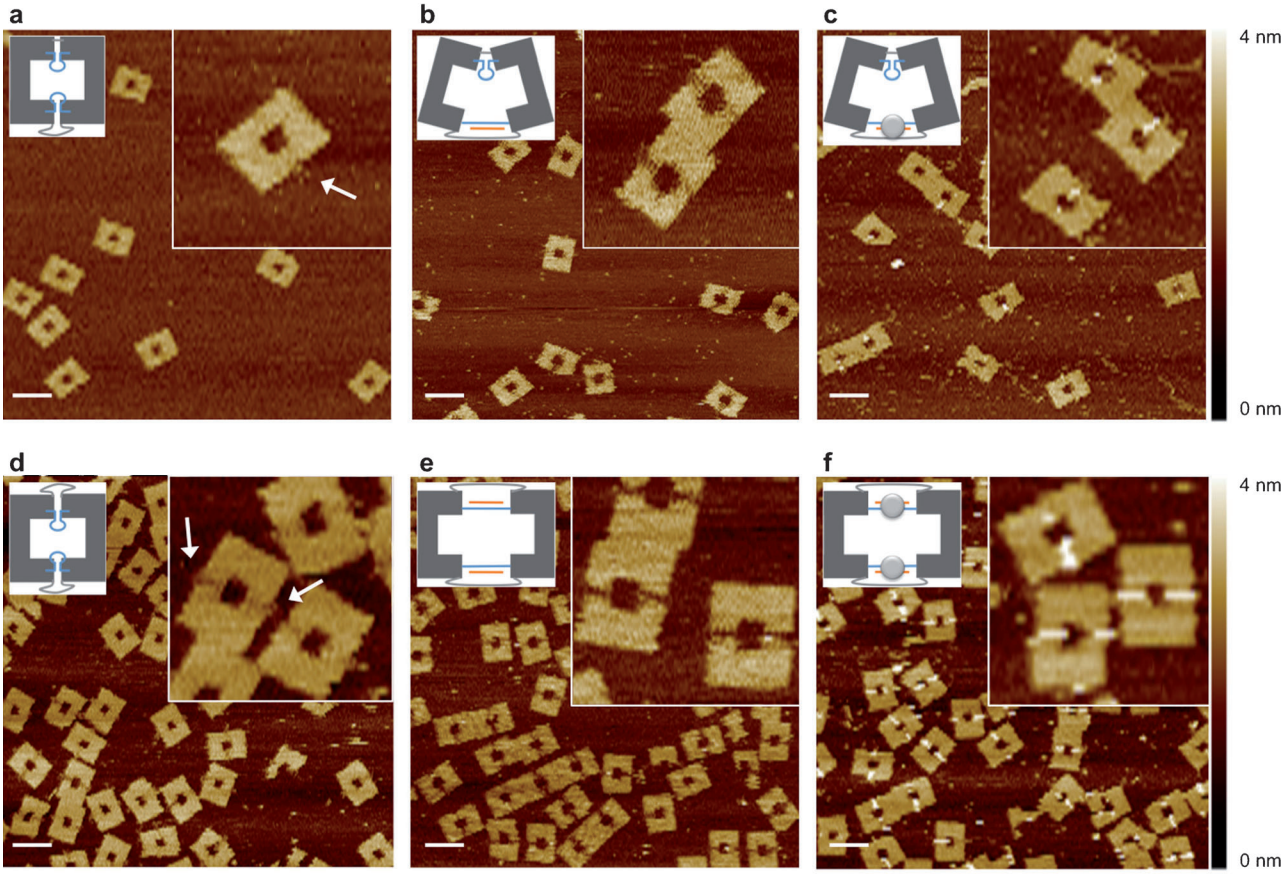

Figure 3. Atomic force microscopy characterization of the tweezer (a–c) and plug (d–f) devices. Note the unpaired region of the scaffold on one or both sides of the closed structures (white arrow in the inset of a and d). The addition of fuels to the initially closed states (a and d for the tweezer and plug system, respectively) triggers the opening of the devices (b and e, respectively). Using biotin-modified fuels followed by direct addition of streptavidin on the mica-adsorbed sample proves the successful hybridization of the fuels to the hairpin motifs of the seam. The appearance of brighter spots preferentially at one (c) or both (f) sides of the central cavity is indicative of a tweezer- or plug-like accessibility, respectively, of the seam sequences. Schematic representations of the devices are also reported. For clarity, the conformation preferentially adopted at the central seam, either above or below the cavity, is indicated by one loop (closed state) or a pair of parallel segments (open state). Similarly, binding of streptavidin molecules to the biotin-modified fuels of the seam is represented by single gray circles. Details of the topographical features of the structures are visible in the insets. Scale bars are 100 nm.

not merely due to a local conformational change at the level of the inner bridge, but are rather indicative of the global structural reconfiguration of the entire DNA origami construct, both on a surface and in solution.

Most interestingly, time-dependent FRET measurements clearly showed that the kinetics of opening and closing processes drastically differed in the four constructs analyzed. The opening of construct I was only achieved after 12 h incubation at room temperature upon annealing with fuel or antifuel strands at moderate temperature (Figure 4b). Lowering the stability of the switchable hairpin motifs, by increasing the ratio of AT versus CG base pairs, considerably accelerated the process, allowing full extension of the construct in only 1 h under ambient conditions (II, see Figure S7 in the Supporting Information). Conformational switching was also possible at ambient temperature with the loop sequence $C_5T_5G_5$ (as in I) by extending the fuel strand with a slightly longer toehold sequence (III, see Figure S8 in the Supporting Information). The extended sequence essentially disfavors formation of a stable hairpin motif, thus facilitating disentanglement of the interacting hairpin loops (see Figure S14 in the Supporting Information).[15] These two designs can be combined (construct IV, see Figure S9 in the Supporting Information) to achieve a 23-fold and 283-fold acceleration of the opening rate as compared to constructs II and III, respectively. The reclosing processes were similarly affected, although to a lesser extent. Altogether, these results clearly indicate that minimal changes in the design of the switchable motifs and/or actuator sequences of the seam greatly affect the free-energy barrier of the opening/closing processes and, consequently, their kinetics. Thus, they provide a valuable strategy for fine-tuning switchable nanochambers.

In conclusion, we have demonstrated that cyclically operating multiple branch migration sites in parallel enables the coordinated movement of a large origami structure. This process can be exploited not only for controlled and reversible switching of the scaffold but also for mechanical transduction onto appended molecular payloads, as shown by altering the distance-dependent energy transfer between two internalized dyes. Preliminary experiments indicate that the

 © 2015 Wiley-VCH Verlag GmbH & Co. KGaA, Weinheim

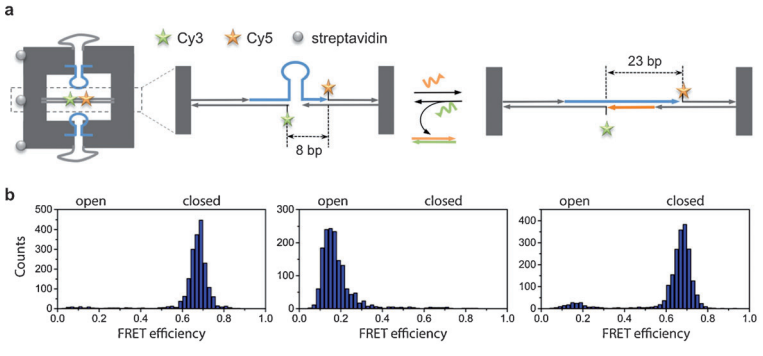

	I	II	III	IV
loop	$C_5T_5G_5$	$C_4T_7G_4$	$C_5T_5G_5$	$C_4T_7G_4$
fuel	$C_5A_5G_5$-CGCG	$C_4A_7G_4$-CGCG	$C_5A_5G_5$-A_5C_5	$C_4A_7G_4$-A_7C_4
antifuel	CGCG-$C_5T_5G_5$	CGCG-$C_4T_7G_4$	G_5T_5-$C_5T_5G_5$	G_4T_7-$C_4T_7G_4$
τ_{op}	12 h	9 min	113 min	0.4 min
τ_{cl}	12 h	17 min	2.8 min	2.1 min

Figure 4. Single-molecule FRET characterization of the plug device. The translational movement of the structure along its *x*-axis was monitored as a change in the FRET signal between a pair of donor (Cy3) and acceptor (Cy5) fluorophores, positioned within the central cavity of the chamber (a). Representative FRET histograms of closed (b, left panel), open (b, center), and reclosed (b, right) DNA origami (construct I) revealed homogeneity of the sample mechanical response as well as completeness and full reversibility of the process. Four different plug constructs (denoted as I, II, III, and IV) with identical labeling positions in the cavity (as in a) and with different sequences of hairpin loops and/or fuel/antifuels strands were examined (see table). The opening (τ_{op}) and closing (τ_{cl}) rate coefficients were evaluated from kinetic experiments (see Figures S7–S9 in the Supporting Information).

inner cavity of the nanochambers can be customized in terms of size and spatial decoration with ligands for protein attachment (see Figures S15 and S16 in the Supporting Information). Compared to previous static scaffolds,[16] those reconfigurable systems provide new options for the dynamic reorganization of proteins. Extending this design principle to 3D structures (see Figure S17 in the Supporting Information) will open the door to more-complex DNA nanodevices that possess not only the peculiar molecular addressability of DNA origami but also the tailorable dynamic properties of small DNA motifs. We anticipate that such architectures can be used for the construction of dynamic DNA–protein assemblies to mimic and explore complex biological processes occurring in living systems.

Received: September 9, 2014
Revised: November 12, 2014
Published online: January 28, 2015

Keywords: atomic force microscopy · DNA origami · self-assembly · single-molecule FRET · structural reconfiguration

[1] a) P. W. Rothemund, *Nature* **2006**, *440*, 297–302; b) S. M. Douglas, H. Dietz, T. Liedl, B. Hogberg, F. Graf, W. M. Shih, *Nature* **2009**, *459*, 414–418; c) W. M. Shih, C. Lin, *Curr. Opin. Struct. Biol.* **2010**, *20*, 276–282; d) T. Tørring, N. V. Voigt, J. Nangreave, H. Yan, K. V. Gothelf, *Chem. Soc. Rev.* **2011**, *40*, 5636–5646; e) B. Saccà, C. M. Niemeyer, *Angew. Chem. Int. Ed.* **2012**, *51*, 58–66; *Angew. Chem.* **2012**, *124*, 60–69.

[2] A. Rajendran, M. Endo, H. Sugiyama, *Angew. Chem. Int. Ed.* **2012**, *51*, 874–890; *Angew. Chem.* **2012**, *124*, 898–915.

[3] a) R. Tsukanov, T. E. Tomov, M. Liber, Y. Berger, E. Nir, *Acc. Chem. Res.* **2014**, *47*, 1789–1798; b) R. Tsukanov, T. E. Tomov, R. Masoud, H. Drory, N. Plavner, M. Liber, E. Nir, *J. Phys. Chem. B* **2013**, *117*, 11932–11942; c) M. B. Scheible, G. Pardatscher, A. Kuzyk, F. C. Simmel, *Nano Lett.* **2014**, *14*, 1627–1633; d) A. Johnson-Buck, N. G. Walter, *Methods* **2014**, *67*, 177–184; e) R. Jungmann, C. Steinhauer, M. Scheible, A. Kuzyk, P. Tinnefeld, F. C. Simmel, *Nano Lett.* **2010**, *10*, 4756–4761; f) G. P. Acuna, F. M. Moller, P. Holzmeister, S. Beater, B. Lalkens, P. Tinnefeld, *Science* **2012**, *338*, 506–510; g) D. Koirala, P. Shrestha, T. Emura, K. Hidaka, S. Mandal, M. Endo, H. Sugiyama, H. Mao, *Angew. Chem. Int. Ed.* **2014**, *53*, 8251–8254; *Angew. Chem.* **2014**, *126*, 8391–8395; h) T. E. Tomov, R. Tsukanov, M. Liber, R. Masoud, N. Plavner, E. Nir, *J. Am. Chem. Soc.* **2013**, *135*, 11935–11941; i) J. Fu, Y. R. Yang, A. Johnson-Buck, M. Liu, Y. Liu, N. G. Walter, N. W. Woodbury, H. Yan, *Nat. Nanotechnol.* **2014**, *9*, 531–536.

[4] a) M. Endo, Y. Katsuda, K. Hidaka, H. Sugiyama, *J. Am. Chem. Soc.* **2010**, *132*, 1592–1597; b) M. Endo, Y. Katsuda, K. Hidaka, H. Sugiyama, *Angew. Chem. Int. Ed.* **2010**, *49*, 9412–9416; *Angew. Chem.* **2010**, *122*, 9602–9606; c) J. Fu, M. Liu, Y. Liu, N. W. Woodbury, H. Yan, *J. Am. Chem. Soc.* **2012**, *134*, 5516–5519; d) S. Yamamoto, D. De, K. Hidaka, K. K. Kim, M. Endo, H. Sugiyama, *Nano Lett.* **2014**, *14*, 2286–2292.

[5] a) E. C. Theil, *Curr. Opin. Chem. Biol.* **2011**, *15*, 304–311; b) C. M. Soto, B. R. Ratna, *Curr. Opin. Biotechnol.* **2010**, *21*, 426–438.

[6] A. J. Douglas, J. A. Young, *Nature* **1998**, *393*, 152–155.

[7] S. M. Nomura, K. Tsumoto, T. Hamada, K. Akiyoshi, Y. Nakatani, K. Yoshikawa, *ChemBioChem* **2003**, *4*, 1172–1175.

[8] C. A. Kerfeld, S. Heinhorst, G. C. Cannon, *Annu. Rev. Microbiol.* **2010**, *64*, 391–408.

[9] a) A. Banerjee, D. Bhatia, A. Saminathan, S. Chakraborty, S. Kar, Y. Krishnan, *Angew. Chem. Int. Ed.* **2013**, *52*, 6854–6857; *Angew. Chem.* **2013**, *125*, 6992–6995; b) R. Crawford, C. M. Erben, J. Periz, L. M. Hall, T. Brown, A. J. Turberfield, A. N. Kapanidis, *Angew. Chem. Int. Ed.* **2013**, *52*, 2284–2288; *Angew. Chem.* **2013**, *125*, 2340–2344.

[10] R. P. Goodman, M. Heilemann, S. Doose, C. M. Erben, A. N. Kapanidis, A. J. Turberfield, *Nat. Nanotechnol.* **2008**, *3*, 93–96.

[11] a) D. Han, S. Pal, Y. Liu, H. Yan, *Nat. Nanotechnol.* **2010**, *5*, 712–717; b) A. Kuzuya, Y. Sakai, T. Yamazaki, Y. Xu, M. Komiyama, *Nat. Commun.* **2011**, *2*, 449; c) S. M. Douglas, I. Bachelet, G. M. Church, *Science* **2012**, *335*, 831–834.

[12] a) M. Marini, L. Piantanida, R. Musetti, A. Bek, M. Dong, F. Besenbacher, M. Lazzarino, G. Firrao, *Nano Lett.* **2011**, *11*, 5449–5454; b) R. M. Zadegan, M. D. Jepsen, K. E. Thomsen, A. H. Okholm, D. H. Schaffert, E. S. Andersen, V. Birkedal, J. Kjems, *ACS Nano* **2012**, *6*, 10050–10053; c) E. S. Andersen, M. Dong, M. M. Nielsen, K. Jahn, R. Subramani, W. Mamdouh, M. M. Golas, B. Sander, H. Stark, C. L. Oliveira, J. S. Pedersen, V. Birkedal, F. Besenbacher, K. V. Gothelf, J. Kjems, *Nature* **2009**, *459*, 73–76.

 © 2015 Wiley-VCH Verlag GmbH & Co. KGaA, Weinheim

[13] a) C. R. Sabanayagam, J. S. Eid, A. Meller, *J. Chem. Phys.* **2005**, *122*, 061103; b) R. Roy, S. Hohng, T. Ha, *Nat. Methods* **2008**, *5*, 507 – 516.
[14] R. Rieger, G. U. Nienhaus, *Chem. Phys.* **2012**, *396*, 3 – 9.
[15] J. S. Bois, S. Venkataraman, H. M. Choi, A. J. Spakowitz, Z. G. Wang, N. A. Pierce, *Nucleic Acids Res.* **2005**, *33*, 4090 – 4095.
[16] a) Y. Suzuki, M. Endo, Y. Katsuda, K. Ou, K. Hikada, H. Sugiyama, *J. Am. Chem. Soc.* **2014**, *136*, 211 – 218; b) Y. Suzuki, M. Endo, C. Cañas, S. Ayora, J. C. Alonso, H. Sugiyama, K. Takeyasu, *Nucleic Acids Res.* **2014**, *42*, 7421 – 7428.

 © 2015 Wiley-VCH Verlag GmbH & Co. KGaA, Weinheim